QUADRUPOLE COUPLING TENSOR FOR ^{11}B IN DATOLITE

QUADRUPOLE COUPLING TENSOR FOR ^{11}B IN DATOLITE

By

KRISHNA CHANDRA LAL

A Thesis

Submitted to the Faculty of Graduate Studies

in Partial Fulfilment of the Requirements

for the Degree

Master of Science

McMaster University

December 1964

MASTER OF SCIENCE (1964)

McMASTER UNIVERSITY
HAMILTON, ONTARIO

TITLE: Quadrupole Coupling Tensor for ^{11}B

AUTHOR: K. C. Lal

SUPERVISOR: Dr. H.E. Petch, Principal, Hamilton College, McMaster University

NUMBER OF PAGES: vi, 47.

ABSTRACT:

The electric quadrupole splitting of the ^{11}B nuclear magnetic resonance signal have been studied in a single crystal of datolite (H Ca B SiO_5) placed in a magnetic field of 6350 Gauss and the methods developed by Volkoff and coworkers have been used to analyse the data.

The space group of datolite, P $2_1/C$, permits two different orientations of the otherwise identical quadrupole coupling tensors existing at the four boron sites in the unit cell. The observed five line ^{11}B ($I = \frac{3}{2}$) spectrum is consistent with the crystal symmetry. The quadrupole coupling constant, eqQ/h, and asymmetry parameter, η, at the unique boron site have been determined as well as the orientation of the principal axes of the electric field gradient tensor. The value of 172±1 Kc/sec found for eqQ/h in datolite is consistent with the overall range of values observed for BO_4 tetrahedra in other crystals.

ACKNOWLEDGEMENTS

It is a pleasure to thank Dr. H.E. Petch for his guidance, encouragement and interest throughout this work.

Thanks are also due to Dr. C. Calvo for many discussions in the field of X-ray crystallography.

This research was supported by grants-in-aid to Dr. Petch from the Defence Research Board of Canada. The author is grateful to the Commonwealth Scholarship and Fellowship Committee of Canada for the award of a scholarship.

CONTENTS

LIST OF FIGURES

LIST OF TABLES

CHAPTER I

INTRODUCTION

The first successful nuclear magnetic resonance experiments using bulk material were carried out independently by Purcell, Torrey and Pound (1946) and Bloch, Hansen and Packard (1946). The former group developed the absorption method in which a single radio frequency coil, placed with its axis perpendicular to the applied magnetic field both excited the sample and detected the nuclear absorption signal. The latter used a transmitter coil to irradiate the sample and a separate receiver coil, placed with its axis perpendicular both to the axis of the transmitter coil and to the direction of the steady magnetic field to receive the nuclear induction signal.

The basis of the resonance method is found in the nature of the interaction of the nuclear magnet with an externally applied field. The Hamiltonian for the interaction of a nucleus of spin quantum number I and magnetic moment μ, with a uniform magnetic field H_o is

$$\mathcal{H} = -\vec{\mu} \cdot \vec{H}_o$$

The components of the magnetic moment are given by 2I+1 values of $\frac{m\mu}{I}$, forming the series, μ, $\frac{(I-1)}{I}\mu$ ..... $-\frac{(I-1)}{I}\mu$, $-\mu$. The energy levels of the nuclear magnet in the magnetic field H_o are therefore given by the (2I+1) values of $-\frac{m\mu H_o}{I}$ and will be a set of equally spaced levels with separation $\frac{\mu H_o}{I}$ between successive levels (Fig. 1(a)). According to the selection rule governing transitions between energy levels,

only those transitions are allowed which cause m to change by ± 1. A quantum of energy can therefore excite transitions between the energy levels if it has the same magnitude as the level spacing

$$h \nu_o = \frac{\mu}{I} H_o$$

where ν_o is the frequency of the electromagnetic radiation supplying the quantum of energy. To excite such transitions in the magnetic resonance experiment, it is necessary to supply radiation with the magnetic vector circularly polarized in a plane perpendicular to the magnetic field. In a typical magnetic field of 5000 gauss the resonance frequency ν_o for most of the nuclei lies in the radio frequency range.

From the theory of Einstein Coefficients (Einstein 1917), the probability of transitions upwards by absorption is equal to the probability of transition downwards by stimulated emission. If the number of nucleii in each energy level were equal, the average rate of transitions up and down would be equal and there would be no net effect on the system. Actually, however, since the nuclear spins are in equilibrium at temperature T_S, the population of the lower level exceeds that of the upper level by the Boltzman factor $\exp\left(-\frac{\Delta E}{KT}\right)$ and due to this excess of population in the lower energy state, there is a net absorption of energy from the R/F field.

If in addition to the magnetic moment $\vec{\mu}$, the nucleus possesses an electric quadrupole moment eQ, it will interact also with a non-vanishing electric field gradient $\nabla\tilde{E}$ at the nuclear site. The total Hamiltonian for the nuclear interaction then becomes

$$\mathcal{H} = -\vec{\mu} \cdot \vec{H}_o + \tilde{Q} \cdot \nabla\tilde{E}$$

where $\tilde{Q} \cdot \nabla\tilde{E}$ represents the interaction of the nuclear quadrupole moment eQ with the electric field gradient $\nabla\tilde{E}$. The electric field gradient is a characteristic of the nuclear environment and hence the crystal structure. When the quadrupole interaction $\tilde{Q}.\nabla\tilde{E}$, is small compared to the magnetic interaction $\vec{\mu} \cdot \vec{H}$, $\tilde{Q} \cdot \nabla\tilde{E}$ can be considered as a perturbation for the calculation of the energy eigen values. The perturbation of the energy levels is illustrated in fig. 1(b) for the case when the quadrupole interaction is sufficiently small that first order perturbation terms alone describe the system accurately, and in fig. 1(c) for the case when the quadrupole interaction is sufficiently large that second order perturbation terms are required for a complete description of the energy levels. The result of this additional interaction is that the 2I+1 nuclear Zeeman levels are shifted by unequal amounts so that they are no longer equidistant. Therefore, the transitions between adjacent magnetic levels no longer involve the same energy, but give rise to a spectrum of 2I distinct n.m.r. lines.

In the case of small quadrupole intereaction where first order perturbation theory alone is sufficient to describe the results, the satellite lines are symmetrically placed about the central line which coincides with the Larmor frequency $\nu_o = \frac{\mu H}{Ih}$. In the case of large quadrupole interaction where second order terms must be considered, the satellites are not symmetrical about ν_o and the central component is displaced from ν_o. Perturbation terms higher than the second are rarely useful.

Figure 1

The quadrupole perturbation of the nuclear Zeeman levels for a nucleus of spin $\frac{3}{2}$. The energy levels are shown at the top and the spectrum obtained from such a system at the bottom of the diagram.

a) No quadrupole intereaction.

b) First order quadrupole intereaction showing the symmetrical splitting of the satellite lines ($\nu''_{3/2}$, $\nu'_{3/2}$).

c) Second-order quadrupole interaction showing the shift of the central component from the Larmor frequency $\nu_o = \frac{\mu H}{Ih}$ and the non-symmetrical splitting of the satellites.

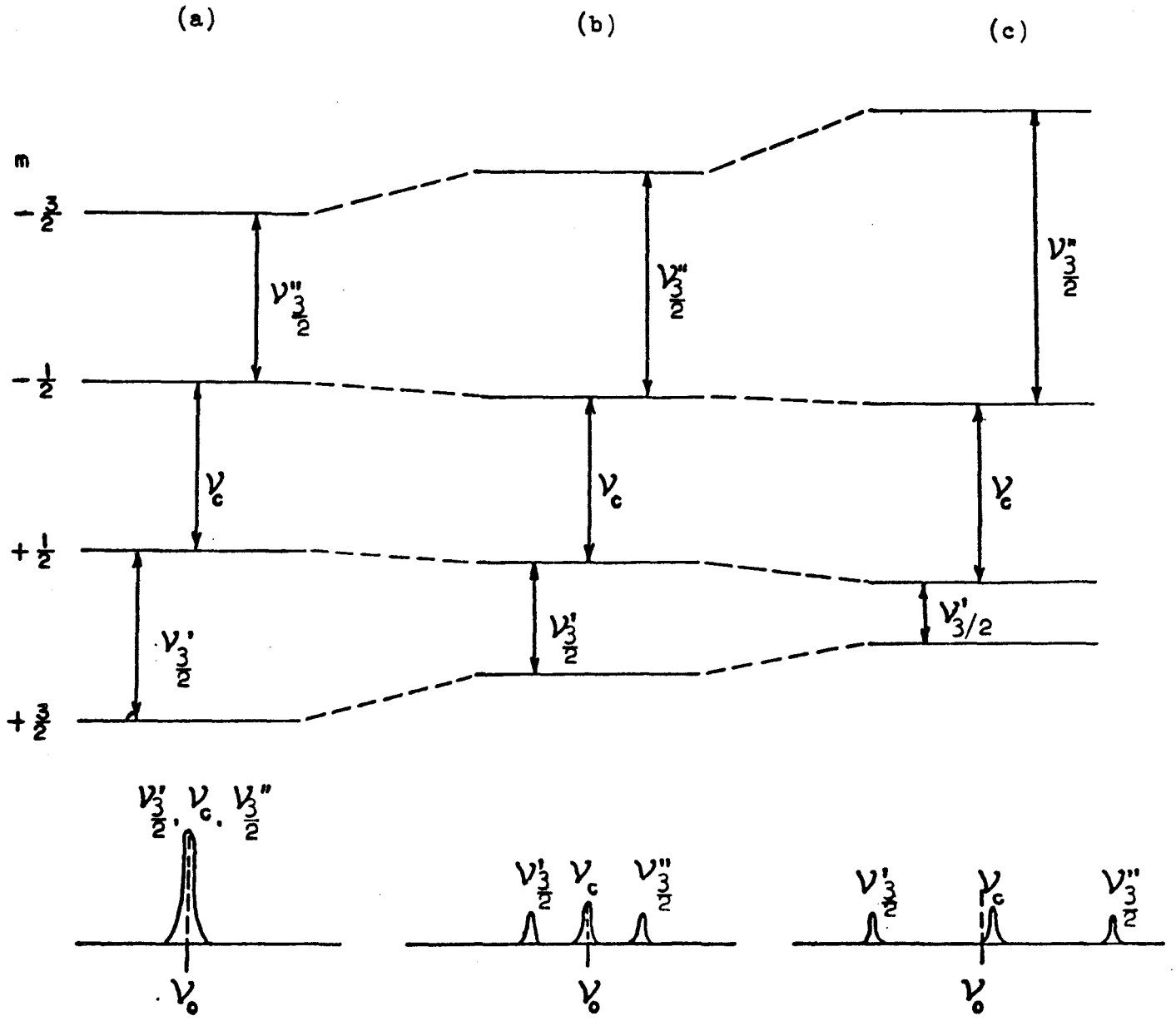
(a)
(b)
(c)
m
$-\frac{3}{2}$
$-\frac{1}{2}$
$+\frac{1}{2}$
$+\frac{3}{2}$
$\nu''_{3/2}$
ν_c
$\nu'_{3/2}$
$\nu'_{3/2}$, ν_c, $\nu''_{3/2}$
ν_0

The first theoretical and experimental investigation of the quadrupole splitting of the n.m.r. lines arising in crystalline solids was carried out by Pound (1960). This work was restricted to crystals in which the nucleii of interest occupied physically identical positions having axial symmetry. Volkoff (1953), Petch, Crana and Volkoff (1953); and Waterman and Volkoff (1955) extended both theory and experimental procedure to the completely general case of several non-identical nucleii in non-axially symmetric positions.

In the hydrated borates, the boron atoms are tightly bound to oxygen atoms in either tetrahedral or triangular coordination. These BO_4 tetrahedra and BO_3 triangles may be expected to exist as discrete insular complexes or to form larger groupings or polyions by sharing oxygen atoms. These polyions may exist as discrete elements in the structure, or they may, by sharing oxygen atoms combine to become structural units in long chains or three dimensional networks. Since the electric field gradient decreases rapidly as the distance from the charges producing the electric field increases, it is reasonable to expect that the quadrupole coupling tensor at a given atomic site to be determined primarily by its nearest neighbours in the structure. Extrapolating from symmetry considerations for the ideal unit, one would predict that the quadrupole coupling constant (q.c.c.) for a ^{11}B nucleus at the centre of a BO_4 tetrahedra would be very small if the tetrahedra existed as a discrete unit in the crystal and somewhat larger if the tetrahedron were linked with other tetrahedra and triangles to form a condensed polyion such as a closed ring. For a ^{11}B nucleus at the centre of a BO_3 triangle, one would predict (1) that the q.c.c. would be

considerably larger than in the case of a tetrahedron, (2) that the value of would be very small and (3) that the z (direction in which the tensor has its maximum component) principal axis would be nearly perpendicular to the plane containing the triangle. This type of interpretation of the gross features of the quadrupole coupling tensor (q.c.t.) existing at boron sites has been very useful in providing information about boron coordinations and about the type of boron-oxygen polyions occurring in the hydrated borates.

Christ (1960); Edwards and Ross (1960) gave a set of rules which seemingly govern the nature of the complex boron oxygen polyions existing in hydrated borate crystals. Following these rules, Christ (1960) has postulated the type of polyions to be found in each of many hydrated borates of unknown crystal structures.

These predictions have been verified in the following single crystal studies:

(i) for discrete BO_4 tetrahedra in teepelite (Ross & Edwards, 1959)

(ii) for two tetrahedron and a triangle in a closed ring in colemanite (Holuj and Petch, 1960)

(iii) for two tetrahedron and a triangle forming a closed ring polyion in inderite (Pennington and Petch, 1960)

(iv) for two tetrahedron and a triangle forming a closed ring polyion in lesserite (Pennington and Petch, 1962)

(v) for polyions made up of two BO_4 tetrahedra and two BO_3 triangles in tincalconite and borax (Cuthbert and Petch, 1963)

The data of Watermann and Volkoff (1955) for kernite shows that polyion contains two tetrahedra and two triangles as in borax in accordance with Christ's prediction with the difference that due to the polymerization of polyions in forming an infinite chain, the polyions are sufficiently distorted to cause the two-field symmetry of the borax polyion lost.

(vi) for BO_4 tetrahedra forming extended chain structure in danburite (Lal and Petch, 1964).

The results of these investigations show that in several of the hydrated borates the ^{11}B quadrupole coupling constant falls approximately within the range 50-100, 300-600 and 2500-2600 Kc/sec for discrete BO_4 tetrahedra, BO_4 tetrahedra in closed ring polyions and BO_3 triangles respectively. Further, for BO_3 triangles, the asymmetry parameter is about 0.1 or less and the z principal axis is perpendicular to the plane of the triangular group.

On the basis of these limited number of observations on hydrated borates, it appeared that it might be possible to distinguish whether tetrahedra are linked to form extended chains or compact ring polyions according to whether the q.c.c. falls into the lower or upper half respectively of the observed range 50-600 Kc/sec. To test this possibility and to verify the general applicability of these results to other boron-containing materials, the ^{11}B quadrupole coupling tensor has been determined in datolite ($HCa\,BSiO_5$), a boro-silicate mineral in which the BO_4 tetrahedra are linked with SiO_4 tetrahedra to form a three-dimensional network (Ito and Mori, 1953).

CHAPTER II

THEORY

II-1. Introduction

This chapter outlines the theory of the dependence of the nuclear magnetic resonance frequencies in a single crystal on the orientation of the crystal with respect to the uniform magnetic field, $\vec{H}_o$ in which the crystal is kept.

The only important contributions to the total interaction energy of the nucleus with a static electromagnetic field arise through the nuclear magnetic moment, $\vec{\mu}$, and the electric quadrupole moment, $\tilde{Q}$, which interact with the total magnetic field and electric field gradients respectively at the nucleus.

The Hamiltonian operator for the interaction of a nucleus at a given site with the static electromagnetic fields is given by

$$\mathcal{H} = -\vec{\mu} \cdot \vec{H}_o + \tilde{Q} \cdot (\nabla \tilde{E}) \qquad (2.1)$$

For a particular nucleus in a particular situation, the energy due to the interaction of its quadrupole moment tensor, $\tilde{Q}$, with the electric field gradient tensor, $\nabla \tilde{E}$, existing at its site, is not necessarily small as compared to the interaction of its magnetic moment, $\vec{\mu}$, with the external magnetic field, $\vec{H}_o$. However, this discussion, following Pound (1950), Bersohn (1952), and Volkoff (1953) is restricted

to cases where the nuclear electric quadrupole interaction, $\tilde{Q} \cdot \nabla \tilde{E}$, is weak as compared to the nuclear magnetic interaction, $\vec{\mu} \cdot \vec{H}_o$, but large as compared with magnetic dipole-dipole interactions, which are neglected so that the term $\tilde{Q} \cdot \nabla \tilde{E}$ can be regarded as perturbation on the magnetic interaction $\vec{\mu} \cdot \vec{H}_o$.

II-2. The Nuclear Electric Quadrupole Hamiltonian

Consider a nucleus of atomic number Z whose total electric charge Ze is distributed over the nuclear volume with a density $\rho(\bar{x})$ at the point $\bar{x}$. Let $\phi(\bar{x})$ be the electrostatic potential arising from all charges other than those of nucleus under consideration.

The orientation-dependent part of the Hamiltonian for the interaction of the nuclear charge distribution with the electrostatic potential is given by Cohen and Reif (1957)

$$\mathcal{H} = \frac{1}{6} \sum_{j,k} Q'_{jk} \left(\frac{\partial^2 \phi}{\partial x_j \, \partial x_k}\right)_0 + \cdots\cdots \qquad (2.2)$$

The subscript zero indicates that the components of the electric field gradient tensor $\phi_{jk} = \frac{\partial^2 \phi}{\partial x_j \, \partial x_k}$ are to be evaluated at the centre of the nuclear site. $Q'_{jk} = \int \rho(\bar{x}) \, x_j \, x_k \, d^3\bar{x}$ is the electric quadrupole moment tensor. Both Q'_{jk} and ϕ_{jk} are second rank symmetric tensors. It is advantageous to define a simpler tensor Q_{jk} which is not only symmetric but also traceless

$$Q_{jk} = 3Q'_{jk} - \delta_{jk} \sum_e Q'_{ee}$$

The Hamiltonian then becomes

$$\mathcal{H} = \frac{1}{6} \sum_{jk} Q_{jk} \phi_{jk} + \tfrac{1}{2} (\Sigma_e Q_{ee'}) (\Sigma_j \phi_{jj}) \qquad (2.3)$$

The last term involves only traces, thus it is independent of nuclear orientation and can be neglected. We are then interested only in matrix elements of the form $\langle Im' | Q_{jk} | Im \rangle$ diagonal in I. Using the components of nuclear spin, whose matrix elements are well known, it is possible to construct a tensor whose components are proportional to Q_{jk}. Then

$$\langle Im' | Q_{jk} | Im \rangle = C \langle Im' | \tfrac{3}{2} (I_j I_k + I_k I_j) - \delta_{jk} I^2 | Im \rangle \phi_{jk} \qquad (2.4)$$

where $C = \frac{eQ}{I(2I-1)}$ and

eQ is the expectation value of the nuclear quadrupole moment in the state characterized by the magnetic quantum number m = I and is called the electric quadrupole moment.

Considering the nuclear spin to be quantised along the z direction and using the matrix elements of spin components $I_\pm = I_x \pm I_y$, the matrix elements of the quadrupolar Hamiltonian can be written as

$$\langle Im | \mathcal{H}_Q | Im \rangle = \frac{eQ}{4I(2I-1)} \left[3m^2 - I(I+1) \right] (\nabla \tilde{E})_0$$

$$\langle I(m\pm1) | \mathcal{H}_Q | Im \rangle = \frac{eQ}{4I(2I-1)} (2m\pm1) \left[(I \mp m)(I \pm m + 1) \right]^{\frac{1}{2}} (\nabla \tilde{E})_{\mp 1}$$

$$\langle I(m\pm2) | \mathcal{H}_Q | Im \rangle = \frac{eQ}{4I(2I-1)} \left[(I \mp m)(I \mp m - 1)(I \pm m + 1)(I \pm m + 2) \right]^{\frac{1}{2}} (\nabla \tilde{E})_{\mp 2}$$

$$\langle m' | \mathcal{H}_Q | m \rangle = 0 \text{ for } |m' - m| > 2 \qquad (2.5)$$

where
$$(\nabla \tilde{E})_0 = \phi_{zz}$$
$$(\nabla \tilde{E})_{\pm 1} = \phi_{xz} \pm i\phi_{yz}$$
$$(\nabla \tilde{E})_{\pm 2} = \tfrac{1}{2}(\phi_{xx} - \phi_{yy}) \pm i\phi_{xy} \qquad (2.6)$$

II-3. Energy levels and allowed transitions

In the case where $\tilde{Q}.\nabla\tilde{E}$ is much smaller than $-\vec{\mu}.\vec{H}_o$, the energy eigen values for the Hamiltonian

$$\mathcal{H} = -\vec{\mu}.\vec{H}_o + \mathcal{H}_Q$$

can be calculated by using the perturbation theory which gives the following relations for the differences between the transition frequencies

$$\Delta\nu = \nu_m'' - \nu_m' = \frac{3(2m-1)}{2I(2I-1)} \left(\frac{eQ}{h}\right) (\nabla\tilde{E})_o$$

$$\bar{\nu} - \nu_o = \frac{\nu_m''+\nu_m'}{2} - \nu_o = \left(\frac{eQ}{h}\right)^2 \frac{1}{2\nu_o[2I(2I-1)]^2} \cdot$$

$$\left\{\left[2I(I+1) - 1 - 2(3m^2-3m+1)\right] \left|(\nabla\hat{\tilde{E}})_{\pm 2}\right|^2 \right.$$

$$\left. - \left[4I(I+1) - 1 - 8(3m^2-3m+1)\right] \left|(\nabla\hat{\tilde{E}})_{\pm 1}\right|^2 \right\} \qquad (2.7)$$

$$\nu_c - \nu_o = \frac{1}{2\nu_o[2I(2I-1)]^2} \left(\frac{eQ}{h}\right)^2 \left\{\left[2I(2I+1) - \frac{3}{2}\right] \left|(\nabla\hat{\tilde{E}})_{\pm 2}\right|^2 \right.$$

$$\left. - \left[4I(I+1) - 3\right] \left|\nabla\hat{\tilde{E}}_{\pm 1}\right|^2 \right\}$$

$\nu_o = \left|\frac{\mu H_o}{Ih}\right|$ is the resonance frequency of the unperturbed system and $\bar{\nu} = \frac{\nu_m''+\nu_m'}{2}$ is the centroid of the satellite pair ν_m'' and ν_m'.

For a nucleus with a half integral spin I, the spectrum of resonance signals consist of a central component at ν_c from transitions between the $m = \frac{1}{2}$ levels and $(I-\frac{1}{2})$ pairs of satellites at ν_m'' and ν_m' from transitions $m \rightleftharpoons m-1$, and $-(m-1) \rightleftharpoons -m$ with $I \geqslant m \geqslant \frac{1}{2}$. In the case of integral spin I, there is no central component but there are I

pairs of satellites. Eq.(2.7) shows that the separation of satellites $\Delta\nu$ is independent of the second order perturbation terms. Further neglecting, third and higher order terms, $\Delta\nu$ is independent of ν_o and hence $\vec{H}_o$. The separations of the centroid of the satellites, $\bar{\nu}$ and the central component, ν_c from the unperturbed frequency ν_o are entirely dependent upon the second order perturbation terms. Further, the separations $(\bar{\nu} - \nu_o)$ and $(\nu_c - \nu_o)$ are inversely proportional to ν_o and hence, $\vec{H}_o$. If the second order perturbation terms are negligible, the central component coincides with the unperturbed frequency (i.e. $\nu_c - \nu_o = 0$), also the satellite lines, ν_m'' and ν_m' are symmetrically situated above and below the central component, (i.e. $\bar{\nu} - \nu_o = 0$). However, if the quadrupole interaction is so large that the second order terms are no longer negligible, the above equations show that the centroid of the satellite lines, $\bar{\nu}$ and the central component, ν_c, no longer coincide with ν_o.

II-4. The Electric Field Gradient Tensor

The electric field gradient tensor $\nabla\tilde{E} = \sum_{j,k=1}^{3} \phi_{j,k}$ is of the second rank

$$\begin{pmatrix} \phi_{XX} & \phi_{XY} & \phi_{XZ} \\ \phi_{YX} & \phi_{YY} & \phi_{YZ} \\ \phi_{ZX} & \phi_{ZY} & \phi_{ZZ} \end{pmatrix}$$

where $\phi_{XX} = -\frac{\delta^2\phi}{\delta x^2}$ etc. and ϕ is the electrostatic potential. The tensor is traceless and symmetric.

Since $\tilde{\nabla E}$ is a symmetric tensor it is always possible to transform it to an orthogonal coordinate system (x,y,z) fixed relative to the crystal axes, in which $\tilde{\nabla E}$ is diagonal. With respect to these new axes x,y,z, the so-called principal axes, the tensor takes the form

$$\begin{pmatrix} \phi_{xx} & 0 & 0 \\ 0 & \phi_{yy} & 0 \\ 0 & 0 & \phi_{zz} \end{pmatrix}$$

where $\phi_{xx} + \phi_{yy} + \phi_{zz} = 0$. A convenient choice of the two parameters sufficient for defining this tensor is the following. Without loss of generality one can orient the principal axes so that the z axis lies along the direction of maximum and the x axis along the direction of minimum field gradient, i.e. such that

$$|\phi_{zz}| \geqslant |\phi_{yy}| \geqslant |\phi_{xx}| \qquad (2.8a)$$

ϕ_{zz} is taken as positive and therefore the quantities ϕ_{xx} and ϕ_{yy} must necessarily be negative. Then one defines the 'two parameters' q and η. ϕ_{zz} is the potential arising from all charges other than those of the nucleus under consideration, while q is the potential when the effect of this nucleus on the surrounding charge distribution is also taken into account. Introduction of the charge of this nucleus causes polarization of the other charges making q slightly different from ϕ_{zz}. In the actual experiment the nucleus is always present and as such ϕ_{zz} is replaced by q.

$$\eta = \frac{\phi_{xx} - \phi_{yy}}{\phi_{zz}}$$

With these substitutions the tensor takes the form

$$\begin{pmatrix} -\phi_{zz}\left(\frac{1-\eta}{2}\right) & 0 & 0 \\ & -\phi_{zz}\left(\frac{1+\eta}{2}\right) & 0 \\ 0 & 0 & \phi_{zz} \end{pmatrix} \qquad (2.8b)$$

Eq. (2.8a) and (2.8b) imply that η has the values

$$0 \leqslant \eta \leqslant 1$$

If the field gradient is axially symmetric, $\phi_{xx} = \phi_{yy}$ and $\eta = 0$. Therefore η is called the 'asymmetry parameter' and measures the departure of the field gradient from cylindrical symmetry. If the field gradient is spherically symmetric, $\phi_{xx} = \phi_{yy} = \phi_{zz}$ so that $\phi_{jj} = 0$ and the quadrupole interaction vanishes.

II-5. Quadrupole Coupling Tensor

In the Volkoff scheme of determining q.c.t., a right-hand set of orthogonal axes X, Y, Z fixed relative to the crystal axes are selected. An orthogonal system of laboratory axes x', y', z' is taken in which x' and y' are perpendicular to the external field.

The components of the tensor are determined in the laboratory system (x', y', z') as the crystal is rotated about one axis, say X-axis which is kept along y' axis perpendicular to the magnetic field $\vec{H}_o$. With the appropriate transformation matrix, the relations between the components of the electric field gradient tensor ϕ_{ij} in the (x', y, z') and (X, Y, Z) system are obtained which when substituted in

eq. (2.6) give the values of $\tilde{\nabla}E$ in the (x', y', z') system. Substituting these values in eq. (2.7) yields

$$\Delta\nu_X = \tfrac{1}{2}(2m-1)\left\{ a_X + b_X \operatorname{Cos} 2\theta_X + C_X \operatorname{Sin} 2\theta_X \right\} \quad (2.9)$$

where
$$a_X = K(\Psi_{YY} + \Psi_{ZZ})$$
$$b_X = K(\Psi_{YY} - \Psi_{ZZ})$$
$$c_X = -2K\,\Psi_{YZ} \quad (2.10)$$
$$K = \frac{3}{2I(2I-1)} \quad \text{and}$$
$$\Psi_{ij} = \left(\frac{eQ}{h}\right)\phi_{ij}$$

Ψ_{ij} is called quadrupole coupling tensor. Similar expressions are obtained for $\nu_c - \nu_o$ and $\bar{\nu} - \nu_o$. By cyclically permutting the X, Y, Z suffixes the corresponding expressions for the Y and Z rotations can be obtained.

Three values for each of the diagonal components Ψ_{ii} of the q.c.t. are obtained. These are averaged and with the single values of the non-diagonal component Ψ_{ij} form the complete 3x3 tensor.

Having determined the tensor Ψ_{ij} in the X, Y, Z coordinates we may now refer it to its principal axis (x, y, z). The tensor is diagonalised and the secular determinant may be written as

$$\gamma^3 - a\gamma - b = 0 \quad (2.11)$$

where $a = \Psi^2_{XY} + \Psi^2_{YZ} + \Psi^2_{ZX} - \Psi_{XX}\Psi_{YY} - \Psi_{YY}\Psi_{ZZ} - \Psi_{ZZ}\Psi_{XX}$

$$b = \Psi_{XX}\Psi_{YY}\Psi_{ZZ} + 2\,\Psi_{XY}\Psi_{YZ}\Psi_{ZX} - \Psi_{XX}\Psi^2_{ZY} - \Psi_{YY}\Psi^2_{ZX} - \Psi_{ZZ}\Psi^2_{XY}$$

The roots of the eq. (2.11) are

$$\gamma_n = 2\left(\frac{a}{3}\right)^{\frac{1}{2}} \cos\left(\alpha - \frac{2n\pi}{3}\right), \quad n = 1, 2, 3$$

where $\cos 3\alpha = \frac{b}{2}\left(\frac{a}{3}\right)^{-1.5}$

γ_3 is positive and γ_1 and γ_2 are negative with

$$|\gamma_3| \geq |\gamma_2| \geq |\gamma_1| \text{ and } \Sigma\gamma_i = 0$$

γ_3 is called the quadrupole coupling constant. The direction cosines λ_n, μ_n, ν_n of the principal axes corresponding to γ_n are given by

$$\frac{\lambda_n}{D_{1n}} = \frac{\mu_n}{D_{2n}} = \frac{\nu_n}{D_{3n}} = \frac{\pm 1}{(D^2_{1n} + D^2_{2n} + D^2_{3n})^{\frac{1}{2}}}$$

where

$$D_{1n} = \Psi_{XY}\Psi_{YZ} - \Psi_{ZX}(\Psi_{YY} - \gamma_n)$$

$$D_{2n} = \Psi_{XY}\Psi_{ZX} - \Psi_{YZ}(\Psi_{XX} - \gamma_n)$$

$$D_{3n} = (\Psi_{XX} - \gamma_n)(\Psi_{YY} - \gamma_n) - \Psi^2_{XY}$$

CHAPTER III

APPARATUS AND EXPERIMENTAL PROCEDURE

This chapter briefly describes the nuclear magnetic resonance spectrometer and the experimental procedure necessary for the complete analysis of the n.m.r. absorption spectrum of a single crystal. A more complete description of the spectrometer is given by Datars (1956).

III-1. Nuclear Magnetic Resonance Spectrometer

A block diagram of the spectrometer is shown in Fig. 2. The large static magnetic field, $\vec{H}_o$, is produced by a varian electromagnet with pole pieces 12 inches in diameter and a gap width of 3 inches. The magnet, energised by a stabilised power supply, provided a field with a long and short term stabilities of 2:100,000 and 1:100,000 respectively in the current range from 0.02 to 2 amperes, provided the temperature of the room was held constant. Variations in the field due to temperature changes in the laboratory were compensated by manual adjustment of the current, a proton signal displayed on an oscilloscope served as a field monitor. The field inhomogeneity over the sample volume (approximately 2 c.c.) was such as to cause no significant broadening of the signals from the crystals.

The oscillating detector was of the type described by Volkoff, Petch and Smellie (1952). It consists essentially of a push pull marginal oscillator, two stages of r.f. amplification followed by detection,

Fig. 2. Block diagram of N.M.R. Spectrometer

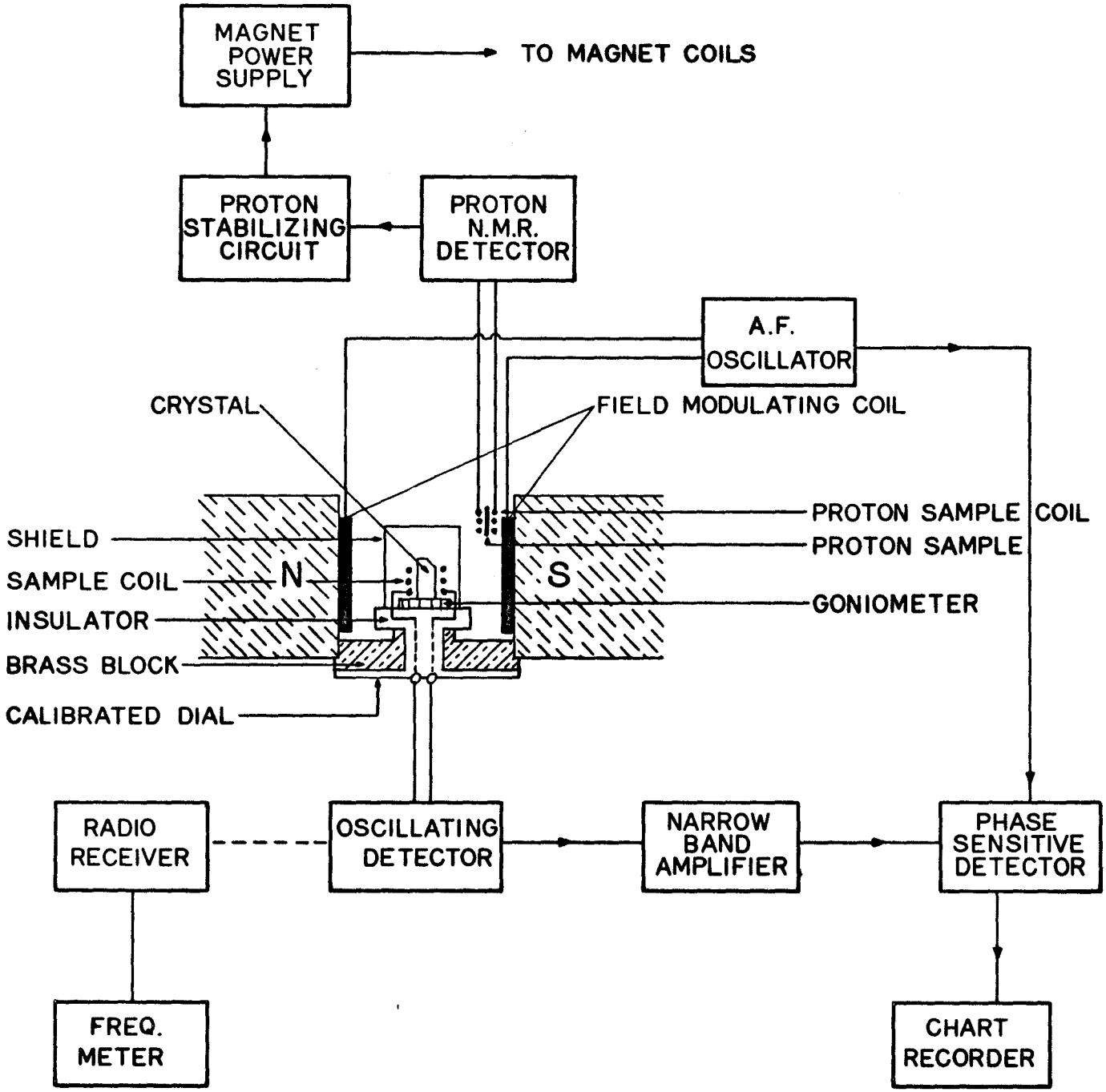
MAGNET POWER SUPPLY
TO MAGNET COILS
PROTON STABILIZING CIRCUIT
PROTON N.M.R. DETECTOR
A.F. OSCILLATOR
CRYSTAL
FIELD MODULATING COIL
PROTON SAMPLE COIL
PROTON SAMPLE
GONIOMETER
SHIELD
SAMPLE COIL
INSULATOR
BRASS BLOCK
CALIBRATED DIAL
N
S
RADIO RECEIVER
OSCILLATING DETECTOR
NARROW BAND AMPLIFIER
PHASE SENSITIVE DETECTOR
FREQ. METER
CHART RECORDER

with d.c. feed back to the oscillator section to maintain the level of the oscillation constant whilst sweeping the frequency. The crystal is held firmly in the tank coil of the oscillator, which is placed between the pole pieces of the electromagnet. This was followed by a stage of A.F. amplification and a narrow band amplifier tuned to the frequency at which the large static magnetic field was modulated. The radio frequency spectrum was scanned by slowly altering the value of the tank circuit capacity using a clock drive followed by a gear system. The frequency sweep rate employed was 150 Kc/hr. Frequencies were measured by mixing the outputs from the marginal oscillator and a frequency meter (General Radio Type 620A) and then listening to the beat frequency with a receiver (Hallicrafters Model SX 62A) and noting when the beat went to zero. The accuracy in the measurement of frequency was about ±0.5 Kc/sec.

The static magnetic field is modulated with an amplitude much smaller than the width of an absorption line (of the order of 3-7 gauss) at a frequency of 210 C/sec. The resonance absorption condition is therefore made repetitive and the output of the oscillator is an audio modulated r.f. carrier. The depth of modulation is proportional, for small modulations, to the slope of the absorption resonance curve. After amplification and rectification in the phase sensitive detector (Schuster, 1951), the output which is approximately proportional to the first derivative of the absorption line is recorded on a recording milliammeter (Westronics Model D 11A).

The sensitivity of the oscillating detector is greatest when the r.f. power is lowest, but the noise level is greater at low r.f. power so a compromise has to be made in selecting the r.f. power.

A photograph of the apparatus used is given on the next page.

III-2. Alignment of the Crystal

For a systematic investigation of a n.m.r. spectrum by the Volkoff method, the orientation of the X, Y, Z system of axes with respect to the laboratory system of axes (x', y', z') in which z' is parallel to the magnetic field $\vec{H}_o$, must be known. The accuracy of the results depend to a large extent on the initial crystal alignment. In this work on datolite which is monoclinic with the angle β nearly equal to 90°, (β = 90°09'), the orthogonal axes X, Y, Z were chosen parallel respectively to the a, b, c crystallographic axes of the crystal which were located with the help of X-ray precession photographs. The inaccuracy caused by taking Y along the b axis was within the experimental error as this crystal could only be alligned within 20' accuracy. The crystal holder consists of a brass block which could be adjusted by a set of screws to fit tightly between the magnet pole faces and a calibrated dial assembly which rotates in the brass block with its axis of rotation always held perpendicular to $\vec{H}_o$. The dial is calibrated at one degree intervals. A brass Unicam goniometer was attached to the rotor of the crystal holder and the crystal was mounted on the arc system in such a way that the X, Y, Z system of axes coincided as close as possible with the mutually perpendicular axes of rotation of the two goniometer arcs and the rotor shaft. For preliminary alignment, a Griffin and George Cathetometer

Fig. 3. Photograph of the apparatus

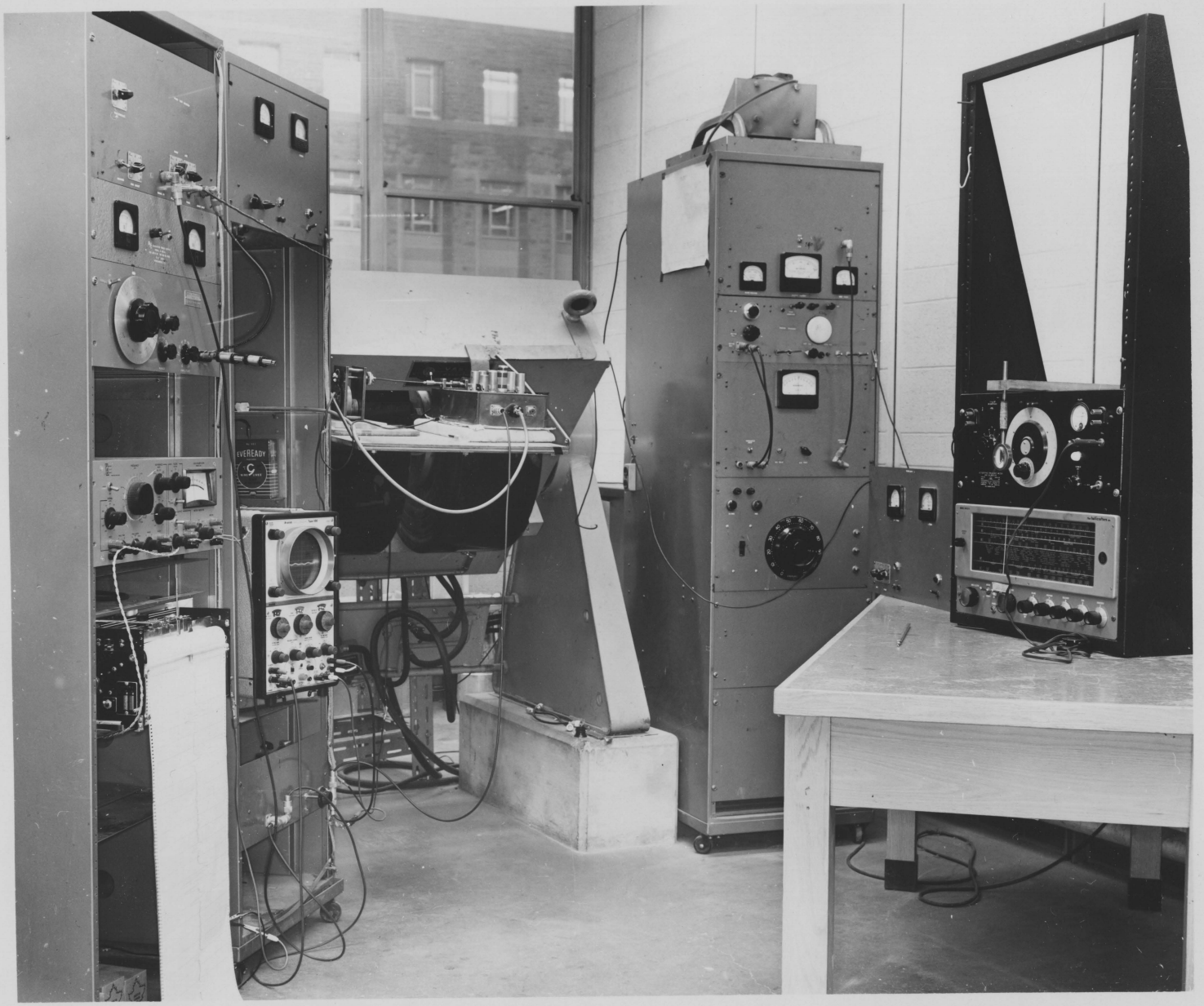
EVEREADY

was used to orient the crystal on the basis of the external features as accurately as possible with the desired axis X, Y or Z parallel to the rotation axes. The crystal face (100) was well defined and a beam of light originating close to the telescope was reflected from the face and back to the telescope which was about 10 feet from the crystal. Another portion of the beam was reflected from a plate of the crystal holder which was made parallel to the rotor axis and fits against the magnetic pole pieces when the holder is placed in the magnet field. Adjustment of the arcs of the goniometer so that both beams were reflected simultaneously into the telescope ensured that the face was perpendicular to $\vec{H}_o$. The $\theta_i = 0$ ($i = X, Y, Z$) reference orientations for the three rotations were also located by this optical method by making use of a well defined edge of the crystal which contained the a-c plane. For the final crystal alignment, n.m.r. spectrum was observed and use was made of the relations describing the orientational dependence of the n.m.r. spectra from symmetry related sites. The Z rotation was first done because in this case two pairs of satellites from the two symmetry related sites were observed whose coalescence could give accurately the 0° and 90° reference positions. The crystal was kept in the magnetic field at an angle of about 10° from the optical zero when two pairs of satellites were observed. The dial was then moved till the symmetry related signals coalesced to give one pair of satellites. At this position of the dial, the arc nearly parallel to the field was adjusted till the signals became sharp and intense. The dial was then turned through 90° and the other arc adjusted to give a similar coalescence. Since this arc movement can upset the first adjustment, the procedure

was repeated until coalescence was obtained at both 0° and 90° showing that at these positions the 2-fold axis is either parallel or perpendicular to the field, because coalescence is observed when a two-fold axis or perpendicular to a mirror plane (in this case b axis) is either parallel or perpendicular to the field. The alignment was checked by noting that the ν'', ν' versus θ curves were symmetrical about 0°, 90° and 180° positions. In the case of the X-rotation only one pair of satellites was observed and the alignment was checked noting that the curves were symmetrical about the 0° and 90° positions and the spectrum at 0° was identical to that at 90° of the Z rotation. For the Y rotation, the two-fold axis was adjusted to be parallel to the rotation axis by altering the arcs to give a coalescence of signals at all θy angles and the zero was found by obtaining the θy and the $\theta y + 90°$ angles at which the signal splittings were equal to those for the equivalent orientations in the X and Z rotations. Moreover, in all the rotations the spectrum at an angle θ was identical to the spectrum at $\theta + 180°$.

III-3. Experimental procedure

For the systematic investigation, the axes X(a), Y(b), Z(c) were held in turn accurately parallel to the axis of rotation of the calibrated dial assembly and the ^{11}B n.m.r. spectrum was recorded at 15° intervals from 0° to 360°. In some regions of the rotations, the spectrum had to be recorded at smaller angular differences to remove uncertainties in the identification of certain lines. In the X, Y and Z rotations the reference position $\theta = 0$ was taken when Y, Z and X, respectively, were

parallel to $\vec{H}_o$. The resonance frequencies of related lines were averaged over all the equivalent orientations to give average values of $\Delta\nu = \nu'' - \nu'$ for the two distinguishable sites. This data was analysed by the 12-point method of Wittaker and Robinson (1942) to yield the Fourier coefficients. The Fourier coefficients thus obtained permitted the quadrupole coupling tensor for each site to be evaluated. Finally the q.c.t. for each site was diagonalised to yield the quadrupole coupling constant and the direction cosines of the principal axes relative to the X, Y, Z system of axes. The calculations were carried out on the I.B.M. 7040 computer system.

CHAPTER IV

RESULTS

IV-1. Crystal data

Datolite is a basic silicate of calcium and boron, Ca $B(SiO_4)(OH)$. It occurs in the form of monoclinic prismatic crystals which are nearly equidimensional in the three axial directions and often complex in development (Fig. 4). It is characterized by its glassy luster, pale green colour, and its crystals with many usually irregularly developed faces (Dana).

The crystallographic data (Ito and Mori, 1953) is as follows:

Monoclinic:	space group $P\ 2_1/C\ (C_{2h}^5)$
Cell dimensions:	$a = 4.84 \pm 0.005$ A°
	$b = 7.60 \pm 0.01$ A°
	$c = 9.62 \pm 0.01$ A°
	$\beta = 90°09'$
Cell contents:	$4(H\ Ca\ B\ SiO_5)$

The structure may be conveniently described as superimposed complex sheets of linked oxygen and O-OH tetrahedra around silicon and boron atoms respectively. In building up the sheet, SiO_4 and a BO_4 tetrahedra alternate and form a ring of four tetrahedra on the one hand and one of eight tetrahedra on the other (Fig. 4). This mode of tetrahedral linkage is broadly the same as those found in other silicate minerals. The sheets are extended indefinitely parallel to (100) and

held solidly together by calcium atoms which have as nearest neighbours six oxygen atoms and two OH groups.

A crystal was removed from a matrix containing many crystals of datolite on its surface. This sample was from West Paterson, New Jersey, U.S.A. The crystal selected had a well defined (100) face and edges which were of much help in the alignment of the crystal. The axes, face (100) and the space group of the crystal were confirmed by X-ray precession photographs. (International Tables for X-ray crystallography.)

IV-2. Crystal Symmetry and the N.M.R. Spectra

The unit cell of datolite contains four boron atoms and it has a centre of symmetry. This means that in a general orientation of the crystal in the magnetic field at most two pairs of satellites can be observed. Further the crystal is monoclinic (space group $P\ 2_1/C$) with the b crystallographic axis as two-fold screw axis and a-c plane is a symmetry plane. The translational symmetry can not be detected in the n.m.r. experiment. As such, the spectrum for the rotation about b axis should consist of only one pair of satellites due to the coalescence of the lines from the two sites related by the 2-fold axis. For rotation about the axis a or c, the spectrum should consist of two pairs of satellites which should reduce to only one pair at the positions in which the two-fold axis b is either parallel or perpendicular to the field. Further, the spectrum about a and c rotations must be symmetrical about the coalescence points 0°, 90°, 180° and 270° positions.

Fig. 4(a). Crystal habit normally exhibited by datolite.

Fig. 4(b). The structure of datolite. Ca atoms are shown by circles. SiO_4 tetrahedra are shaded and BO_4 tetrahedra not shaded. Rings of four tetrahedra are singled out and drawn in projection and in perspective so as to make the reading of the figure easier.

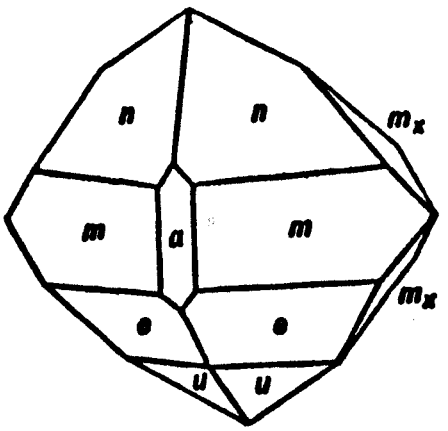

(a) Datolite-crystal habit

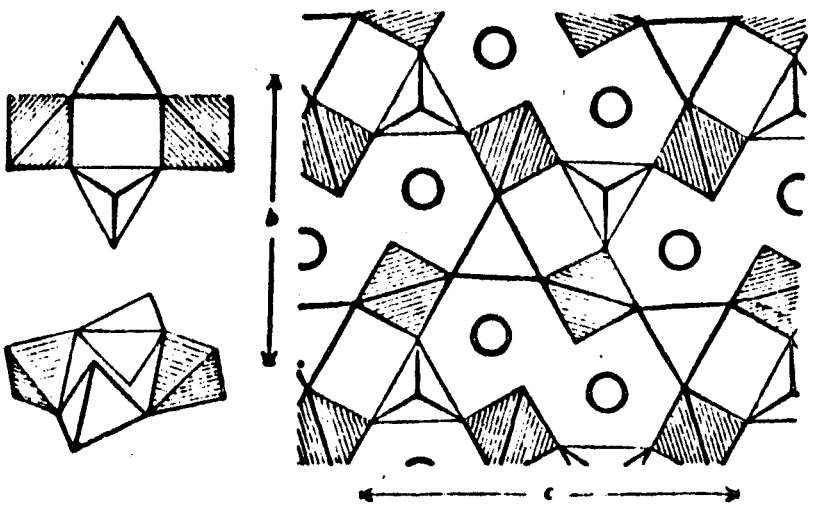

(b) Datolite-crystal structure

The unit cell of datolite has four boron sites, say, K_1, K_2, K_3 and K_4. Assume that K_1 is related to K_3 and K_2 to K_4 by the centre of symmetry and that K_1 and K_2 are related by the 2-fold screw axes.

Since in the experiment K_1 and K_2 will always appear identical with K_3 and K_4 respectively so for simplicity the discussion is limited only to K_1 and K_2 sites.

IV-3. Experimental results

The complete ^{11}B spectrum was observed to consist of five lines centered about 8.688 Mc/sec., whose frequencies depended on the crystal orientation with respect to $\vec{H}_o$. The lines were symmetrically situated about the central line which within experimental error coincided with the calculated frequency ν_o. When one of the axes was either perpendicular or parallel to the field $\vec{H}_o$, only two lines in addition to the central line were observed showing the presence of only one unique site. The frequencies of these lines were measured at 15° intervals from 0° to 360° for a rotation about each of the a, b and c axes and the frequencies of these lines were averaged over all equivalent orientations. The rotation angles for the X, Y and Z rotations were measured from the position at which the Y, Z and X axes, respectively, were parallel to the magnetic field direction. The resonance frequencies are tabulated in Tables, 1, 2, 3 and plotted in Figs. 6, 7, 8. A chart recording of the spectrum is given in Fig. 5. The average values for $\nu''_{3/2} - \nu'_{3/2}$ for the two distinguishable sites which have been denoted by K_1 and K_2 are shown in Fig. 9 and tabulated in Table 4. At some angles certain lines could not be measured as they were superimposed

by the intense central signal. In such cases the separation $\nu'' - \nu'$ was calculated by taking the frequency differences at the measured angles and fitting the curve

$$\nu'' - \nu' = a + b \text{ Cos } 2\theta + c \text{ Sin } 2\theta$$

by the least square method. These data were analysed to give the Fourier coefficients a, b and c of eq. (2.10) and are given in Table-5.

The a, b, c coefficients were used to calculate the components of the q.c.t. in X, Y, Z coordinate system which are recorded in Table-6. These tensors were diagonised to give the values of q.c.c., asymmetry parameter listed in Table-7, and the direction cosines of the principal axes of the q.c.t. given in Table-8.

Fig. 5. Chart recording of the n.m.r. spectrum in datolite for

(a) X-rotation at $\theta_X = 30°$

(b) Y-rotation at $\theta_Y = 60°$

(c) Z-rotation at $\theta_Z = 105°$

(d) General orientation of the crystal in the magnetic field.

The frequency scale is approximately 6 Kc/sec. per chart division.

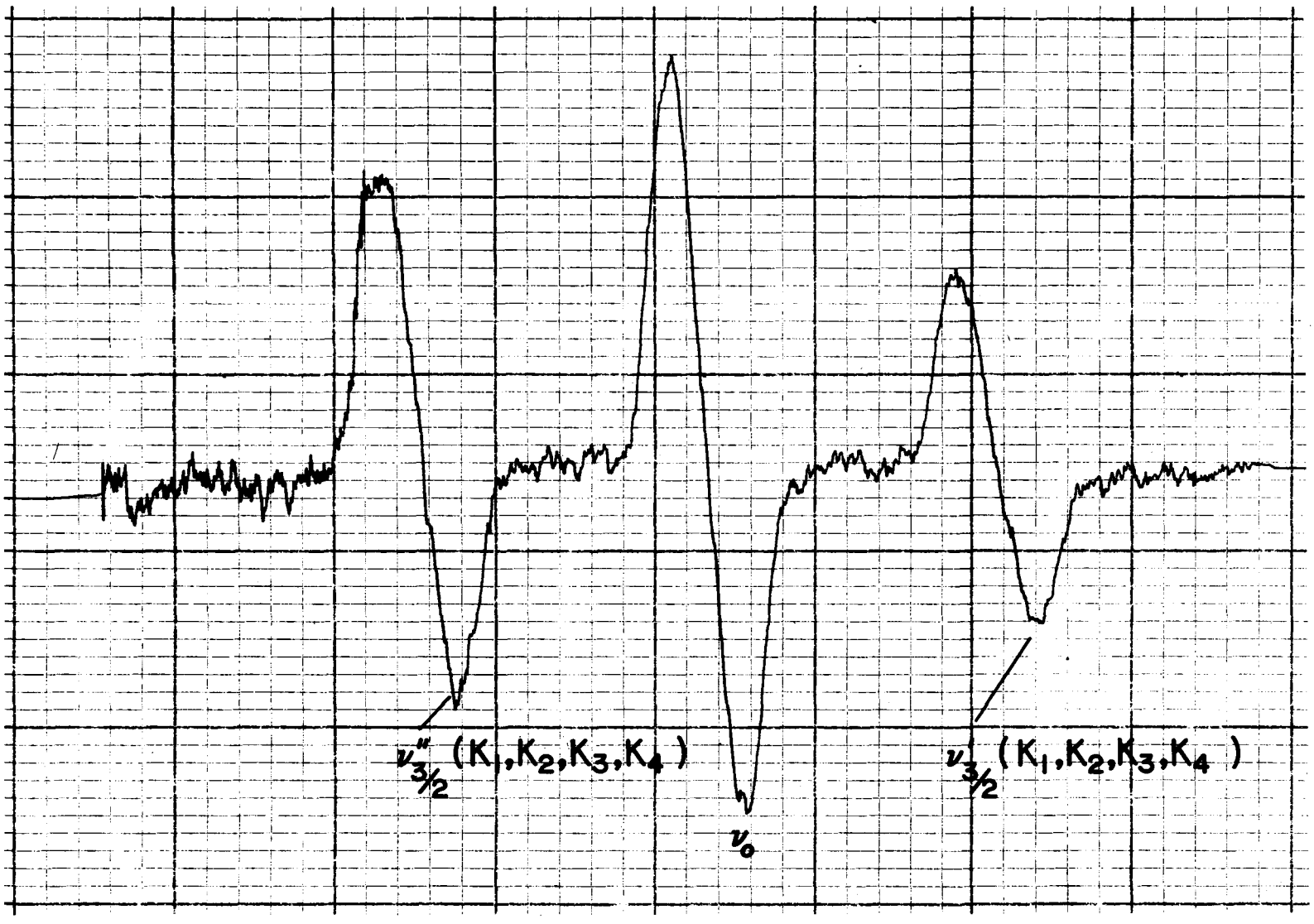
$\nu''_{3/2}(K_1,K_2,K_3,K_4)$
ν_0
$\nu'_{3/2}(K_1,K_2,K_3,K_4)$

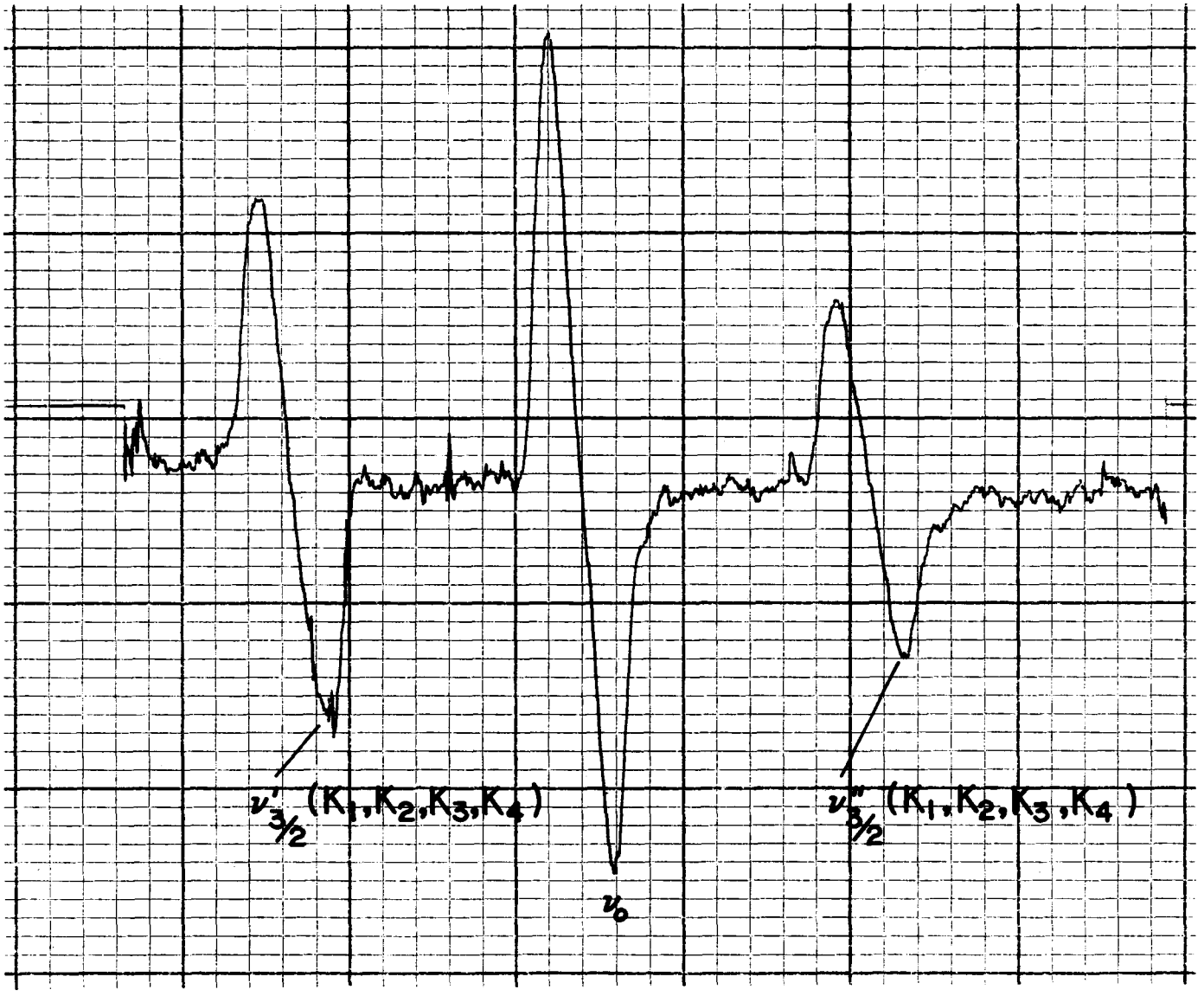
$\nu'_{3/2}(K_1,K_2,K_3,K_4)$
ν_0
$\nu''_{3/2}(K_1,K_2,K_3,K_4)$

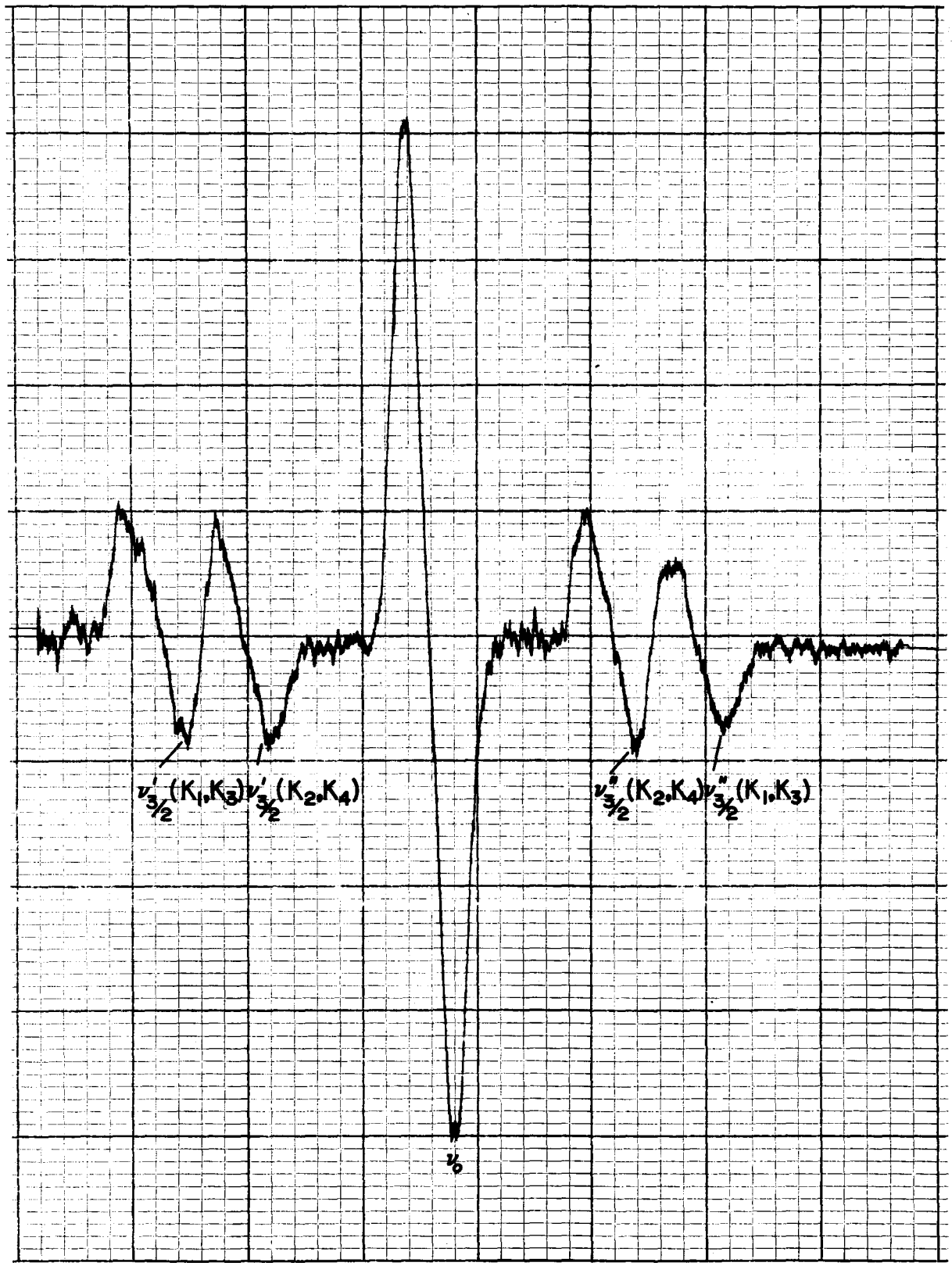
$\nu'_{3/2}(K_1,K_3)$
$\nu'_{3/2}(K_2,K_4)$
ν_0
$\nu''_{3/2}(K_2,K_4)$
$\nu''_{3/2}(K_1,K_3)$

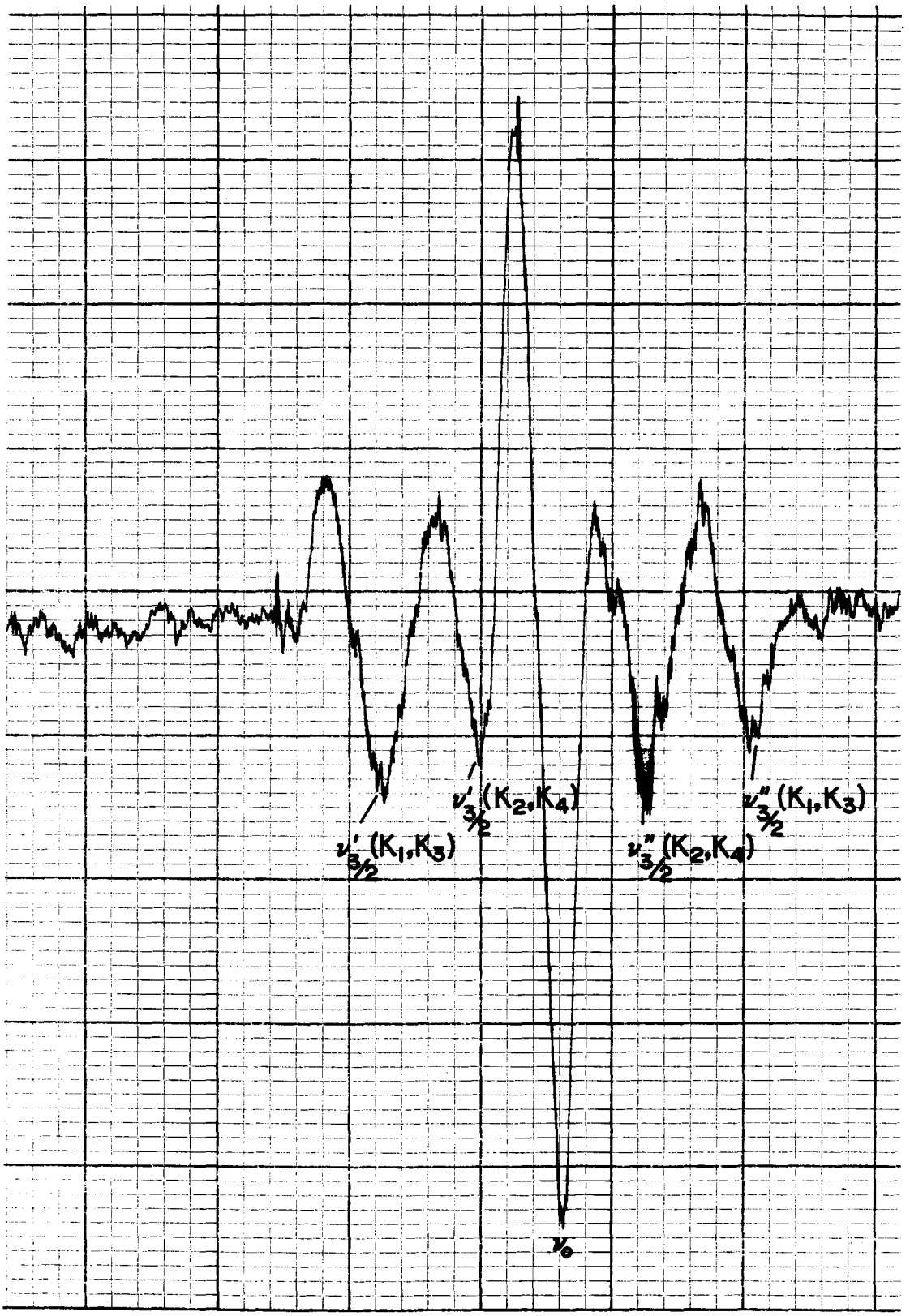
$\nu'_{3/2}(K_1,K_3)$
$\nu'_{3/2}(K_2,K_4)$
$\nu''_{3/2}(K_2,K_4)$
$\nu''_{3/2}(K_1,K_3)$
ν_0

Table-1. Experimental values of the ^{11}B Resonance Frequencies (in Mc/sec.) for the X-rotation of datolite

0°	15°	30°	45°	60°	75°	90°	105°	120°	135°	150°	165°
8.620	8.623	8.633	8.647	8.660	8.670	8.674	8.670	8.660	8.646	8.634	8.623
8.688	8.688	8.688	8.688	8.688	8.688	8.688	8.688	8.688	8.688	8.688	8.688
8.756	8.752	8.743	8.729	8.716	8.706	8.703	8.706	8.715	8.728	8.743	8.752

180°	195°	210°	225°	240°	255°	270°	285°	300°	315°	330°	345°
8.620	8.623	8.633	8.647	8.661	8.670	8.674	8.670	8.660	8.647	8.633	8.624
8.688	8.688	8.688	8.688	8.688	8.688	8.688	8.688	8.688	8.688	8.688	8.688
8.755	8.753	8.743	8.729	8.716	8.706	8.703	8.706	8.716	8.728	8.742	8.751

Fig. 6. Angular dependence of the frequencies of the ^{11}B satellite lines in X-rotation of datolite. The rotation axis X was taken parallel to the crystallographic a axis and the zero reference position was taken in the position in which the b axis was parallel to the magnetic field direction.

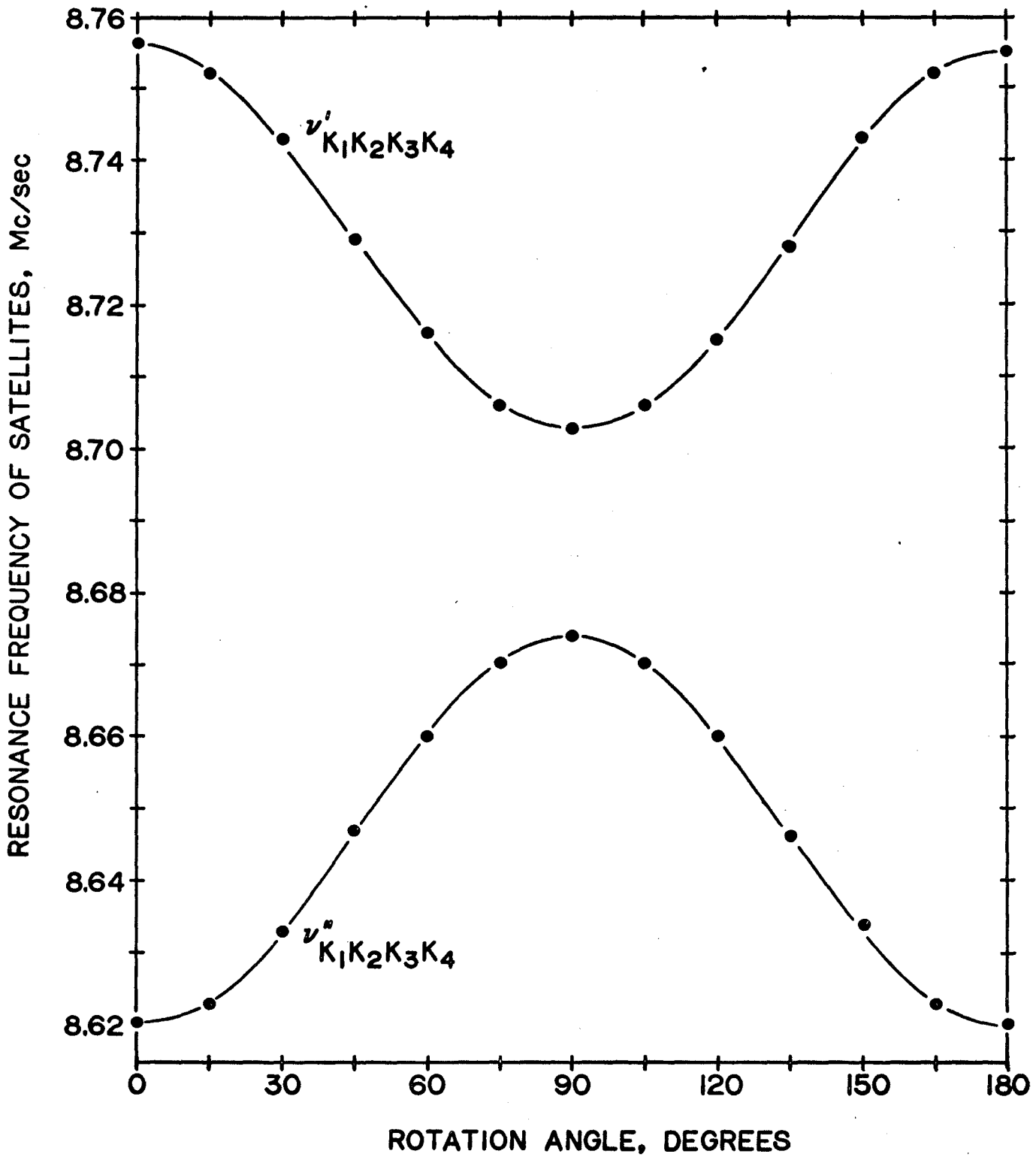
8.76
8.74
8.72
8.70
8.68
8.66
8.64
8.62
RESONANCE FREQUENCY OF SATELLITES, Mc/sec
$\nu'_{K_1K_2K_3K_4}$
$\nu''_{K_1K_2K_3K_4}$
0
30
60
90
120
150
180
ROTATION ANGLE, DEGREES

Table-2. Experimental Values of the ^{11}B resonance frequencies (in Mc/sec.) for the Y Rotation of datolite

0°	15°	30°	45°	60°	75°	90°	105°	120°	135°	150°	165°
8.675		8.674	8.649	8.624	8.609	8.608	8.621	8.640	8.666		8.677
8.689	-	8.689	8.689	8.689	8.689	8.689	8.689	8.689	8.689	-	8.689
8.704		8.704	8.730	8.753	8.768	8.770	8.759	8.740	8.714		8.703

180°	195°	210°	225°	240°	255°	270°	285°	300°	315°	330°	345°
8.674		8.674	8.648	8.624	8.609	8.608	8.618	8.640	8.665		8.676
8.689	-	8.689	8.689	8.689	8.689	8.689	8.689	8.689	8.689	-	8.689
8.703		8.704	8.730	8.754	8.768	8.771	8.759	8.739	8.713		8.703

Fig. 7. Angular dependence of the frequencies of the ^{11}B satellite lines in Y-rotation of datolite. The rotation axis Y was taken parallel to the crystallographic b axis and the zero reference position was taken in the position in which the c axis was parallel to the magnetic field direction.

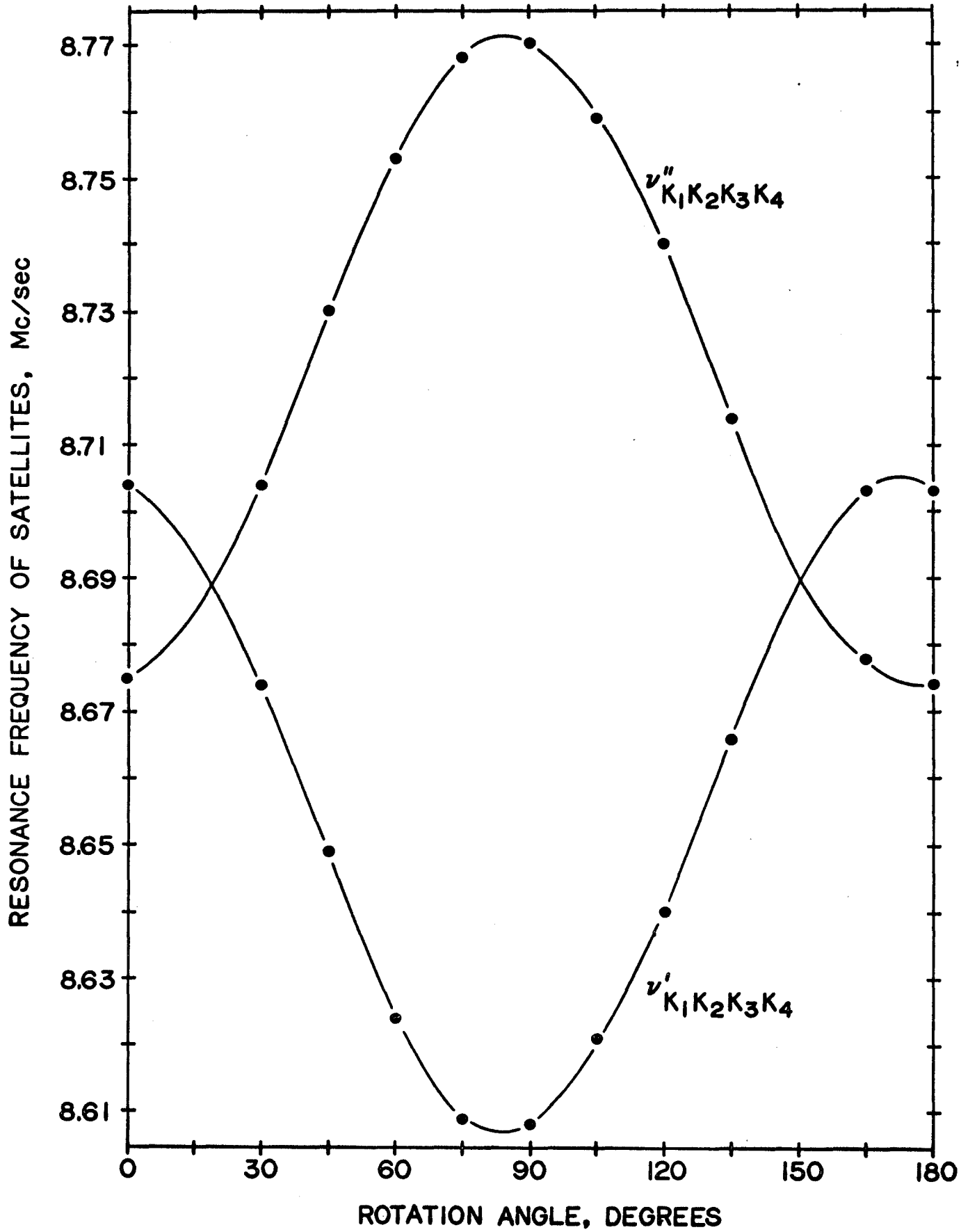
8.77
8.75
8.73
8.71
8.69
8.67
8.65
8.63
8.61
RESONANCE FREQUENCY OF SATELLITES, Mc/sec
$\nu''_{K_1K_2K_3K_4}$
$\nu'_{K_1K_2K_3K_4}$
0
30
60
90
120
150
180
ROTATION ANGLE, DEGREES

Table-3. Experimental values of the ^{11}B resonance frequencies (in Mc/sec.) for the Z rotation of datolite

0°	15°	30°	45°	60°	75°	90°	105°	120°	135°	150°	165°
	8.601	8.623	8.659	8.638	8.619		8.618	8.640	8.660	8.625	8.603
8.605	8.625	8.662	8.674	8.677	8.641	8.620	8.639	8.678	8.673	8.662	8.626
8.687	8.687	8.687	8.687	8.687	8.687	8.687	8.687	8.687	8.687	8.687	8.687
8.770	8.749	8.713	8.701	8.697	8.735	8.755	8.733	8.698	8.702	8.714	8.751
	8.770	8.752	8.716	8.736	8.756		8.756	8.737	8.716	8.753	8.772

180°	195°	210°	225°	240°	255°	270°	285°	300°	315°	330°	345°
	8.602	8.623	8.659	8.640	8.619		8.620	8.639	8.660	8.624	8.602
8.605	8.625	8.661	8.674	8.677	8.641	8.619	8.641	8.677	8.675	8.662	8.625
8.687	8.687	8.687	8.687	8.687	8.687	8.687	8.687	8.687	8.687	8.687	8.687
8.769	8.750	8.714	8.702	8.698	8.733	8.755	8.735	8.697	8.702	8.714	8.750
	8.771	8.754	8.718	8.737	8.756		8.755	8.736	8.717	8.752	8.770

Fig. 8. Angular dependence of the frequencies of the ^{11}B satellite lines in Z-rotation of datolite. The rotation axis Z was taken parallel to the crystallographic c axis and the zero reference position was taken in the position in which the a axis was parallel to the magnetic field direction.

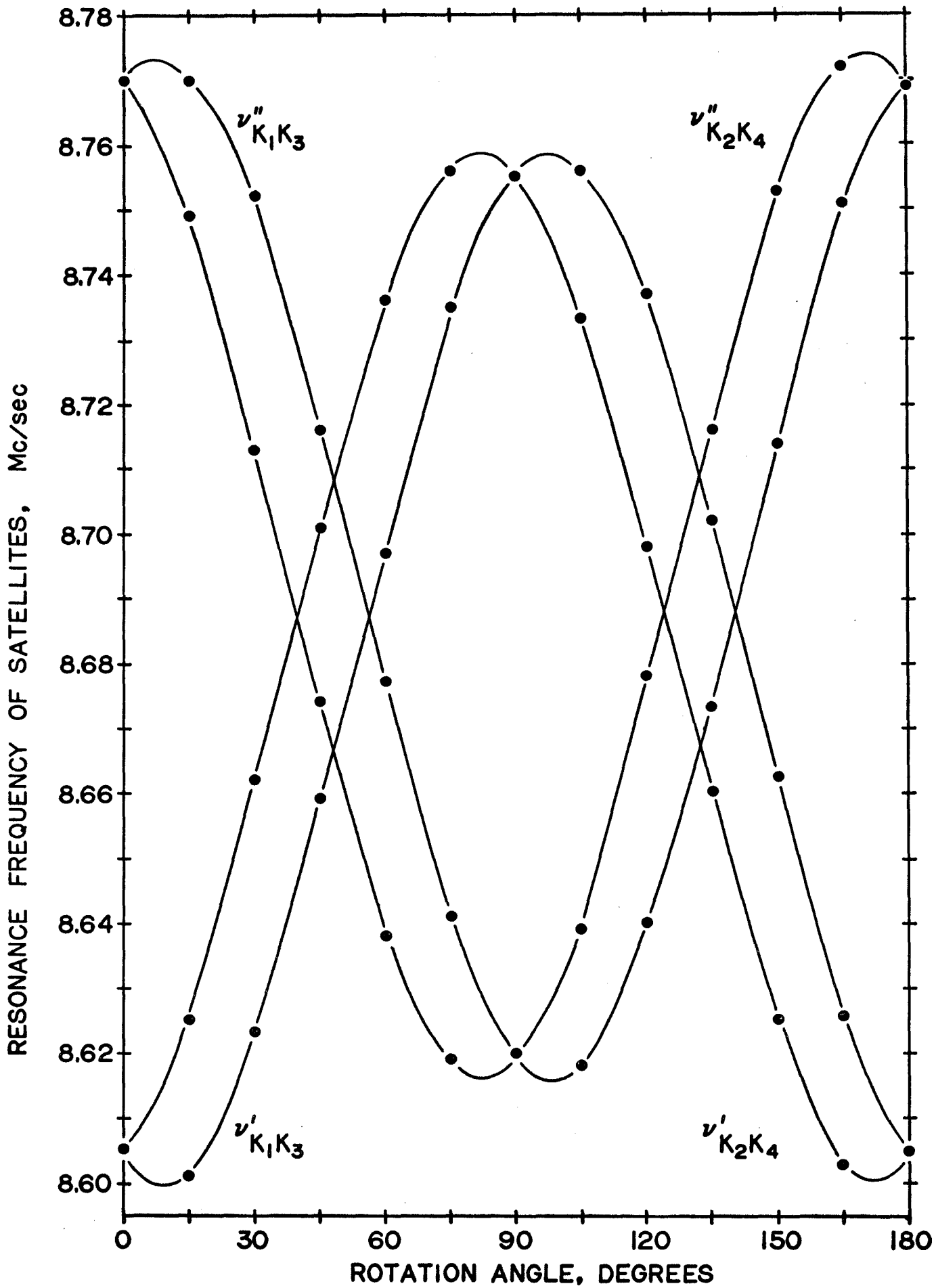
8.78
8.76
8.74
8.72
8.70
8.68
8.66
8.64
8.62
8.60
RESONANCE FREQUENCY OF SATELLITES, Mc/sec
$\nu''_{K_1K_3}$
$\nu''_{K_2K_4}$
$\nu'_{K_1K_3}$
$\nu'_{K_2K_4}$
0
30
60
90
120
150
180
ROTATION ANGLE, DEGREES

Table-4. Frequency Separations (in Kc/sec.) between the ^{11}B satellite lines ($\nu''_{3/2} - \nu'_{3/2}$) in datolite. The signs are relative.

θ	X-rotation Sites K_1, K_2, K_3, K_4	Y-rotation Sites K_1, K_2, K_3, K_4	Z-rotation Site K_1, K_3	Z-rotation Site K_2, K_4
0	-138	- 29	164	164
15	-129	- 9	169	124
30	-110	30	130	52
45	- 82	81	58	- 27
60	- 56	130	- 20	- 97
75	- 36	159	- 93	-137
90	- 29	163	-136	-136
105	- 36	139	-136	- 94
120	- 55	100	- 96	- 20
135	- 82	48	- 28	56
150	-109	3	52	129
165	-129	- 26	124	169

Fig. 9. Angular variation of the frequency difference between the ^{11}B satellite lines in datolite for rotations about the X(a), Y(b) and Z(c) axes. The rotation angles for the X, Y and Z rotations were measured from the positions in which the Y, Z and X axes, respectively, were parallel to the magnetic field direction.

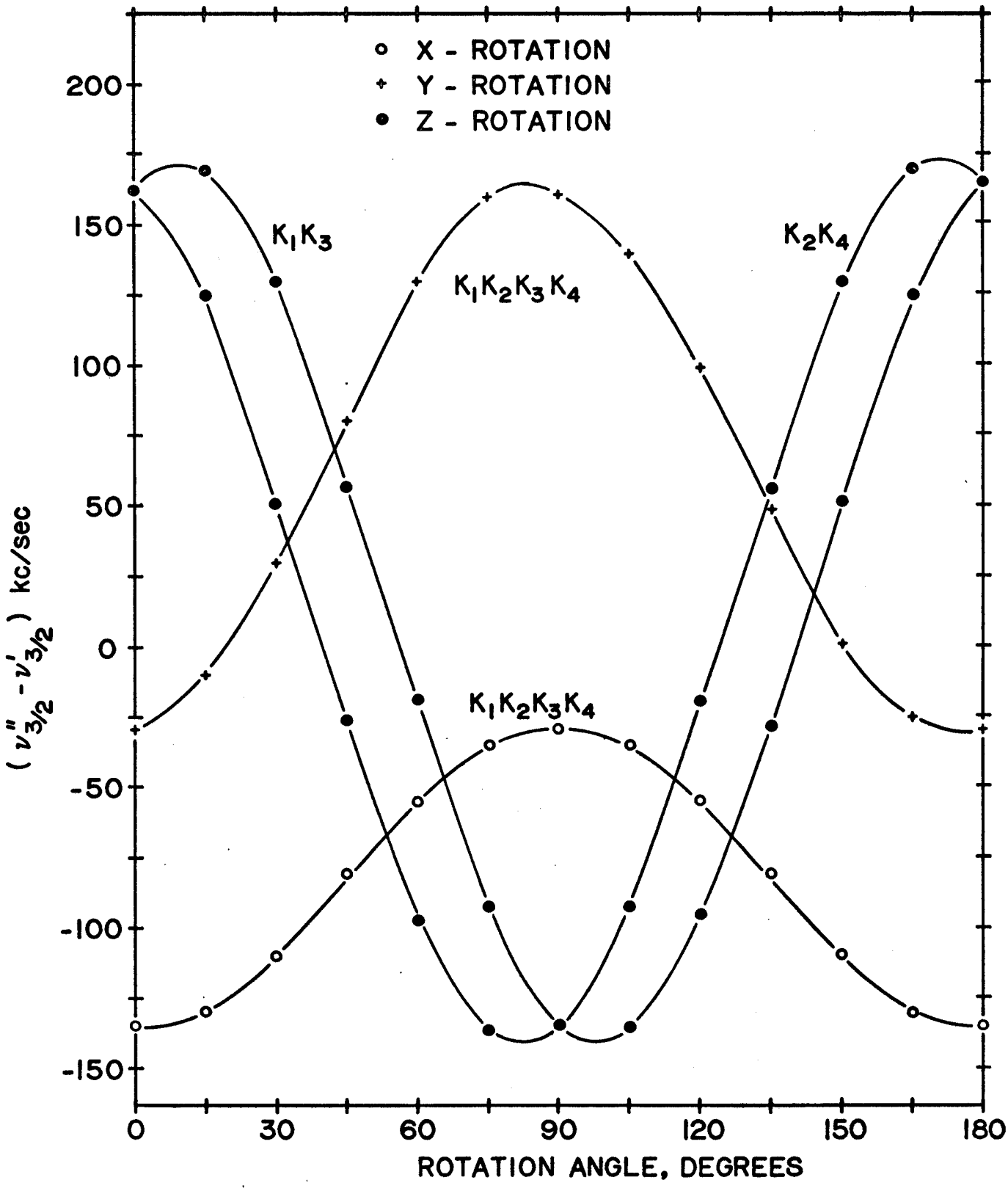
X - ROTATION
Y - ROTATION
Z - ROTATION
200
150
100
50
0
-50
-100
-150
K_1K_3
$K_1K_2K_3K_4$
K_2K_4
$K_1K_2K_3K_4$
$(\nu''_{3/2} - \nu'_{3/2})$ kc/sec
0
30
60
90
120
150
180
ROTATION ANGLE, DEGREES

Table-5. Averaged experimental values of the Fourier coefficients (in Kc/sec.) of the angular variation of the frequency separations ($\nu''_{3/2} - \nu'_{3/2}$) for the ^{11}B satellites arising in datolite. Where alternative signs are given, the upper and lower signs refer to the upper and lower sites, respectively, at the top of the column.

Rotation Fourier coefficient	X K_1, K_2, K_3, K_4	Y K_1, K_2, K_3, K_4	Z K_1, K_3 K_2, K_4
a	-82.33	65.75	15.5
b	-53.51	-96.48	150.32
c	- 0.29	16.81	±43.72

Table-6. Averaged values (in Kc/sec.) for the components of the quadrupole coupling tensor in the X, Y, Z system, Ψ_{ij}, at the ^{11}B sites in datolite. The alternative signs for the off-diagonal term refer to the symmetry related sites K_1, K_3 and K_2, K_4 respectively.

$\Psi_{XX} = 164.24$	$\Psi_{XY} = \mp 43.72$
$\Psi_{YY} = -134.05$	$\Psi_{YZ} = 0.29$
$\Psi_{ZZ} = -30.18$	$\Psi_{ZX} = -16.81$

Table-7. Quadrupole coupling constant and asymmetry parameter at the ^{11}B site in datolite

$\frac{eQq}{h}$ (Kc/s.)	η
172±1	0.633±.015

Table-8. Direction cosines of the principal axes x, y, z of the quadrupole coupling tensors at the ^{11}B sites in datolite. The four combinations of signs refer to the four symmetry related sites K_1, K_2, K_3 and K_4.

Reference axes	Principal axes x	y	z
a	+--+0.079±.007	-++-0.143±.031	+--+0.987±.030
b	++--0.031±.004	++--0.989±.010	++--0.141±.010
c	+--+0.996±.008	-++-0.022±.033	-++-0.083±.032

IV-4. Discussion of Results

Since for ^{11}B the spin I equals $\frac{3}{2}$, the spectrum for a particular boron site in the unit cell should consist of three lines corresponding to the three allowed transitions between the four magnetic levels. The five line spectrum observed in datolite is therefore a superposition of two "simple" three line spectra corresponding to two sites in the unit cell at which the electric field gradients differ in some respect. The central line, counted as one of the five lines, is actually a superposition of two lines of unperturbed frequency ν_o from the two observed sites. The quadrupole interaction being small, the two lines exactly superimpose giving one intense central line. As the crystal is centrosymmetrical, only two of the four boron sites in the unit cell can be separately distinguished in the n.m.r. experiment giving a composite five line spectrum.

The five line spectrum in the Z(c) rotation is reduced to three lines at the 0° and 90° positions when the two-fold axis is either parallel or perpendicular to the field which shows that there is only one unique ^{11}B site in datolite. The q.c.t. at the distinguishable sites must be identical in magnitude and differ only in the orientation of the principal axes.

In the X(a) rotation it would appear from symmetry considerations alone that two pairs of satellites should be observed but in fact only one pair could be resolved. The angular variation of these satellites is symmetrical about 0° and 90° positions. These facts imply that one of the principal axes is very close to being parallel to the c axis while

the other two principal axes must lie almost in the XY plane. Direction cosines of the principal axes, given in Table-8, actually confirm that the x axis is very nearly parallel to the c-axis.

In the Y(b) rotation, which is about a two-fold axis, one pair of satellites, as expected, is observed. In this case the electric field gradient tensors at the two sites, in addition to having identical values, are symmetrically inclined with respect to the two-fold rotation axis and so they are equivalent from the point of view of the perturbation they cause and give rise to the identical spectra.

The small value observed for the ^{11}B q.c.c. in datolite indicates that the boron atoms are in the tetrahedral coordination. Also, the fact that only one unique boron site was observed indicates that the boron and silicon atoms are ordered in the structure at room temperature. This is in agreement with the X-ray results. Hence, it can be concluded that as regards the number of unique sites, the ordering and the coordination of the boron atoms; and the crystal symmetry, the n.m.r. spectrum in datolite is consistent with the structure proposed on the basis of X-ray analysis (Ito and Mori, 1953).

The value of the q.c.c., 172±1 Kc/sec. falls within the range 50-600 Kc/sec. found for tetrahedra in the hydrated borates. In case of danburite, another boro-silicate, Lal and Petch (1964) observed a value 391.8 Kc/sec. for $\frac{eqQ}{h}$ which also lies in the range for hydrated borates. This seems to confirm that $\frac{eqQ}{h}$ for tetrahedra in boro-silicates fall in the same characteristic range as in hydrated borates. However, the BO_4 tetrahedra in danburite and datolite together with the SiO_4 tetrahedra form extended chains while the BO_4 tetrahedra in the hy-

drated borates together with BO_3 triangles form complex ring polyions except in the case of teepelite in which the BO_4 tetrahedra are discrete and the q.c.c. value is only 50 Kc/sec. It appears therefore that the linkage arrangements of the tetrahedra can not be derived from the consideration of the quadrupole coupling constants alone.

BIBLIOGRAPHY

Andrew, E.R. Nuclear Magnetic Resonance (Cambridge University Press 1955).

Bersohn, R. J. Chem. Phys. 20, 1505 (1952).

Bloch, R.; Hansen, W.N. and Packard, M. Phys. Rev. 69, 37 (1946).

Bray, P.J.; Edwards, J.O.; O'Keefe, J.G.; Ros, V.F. and Tatsuzaki, I. Jour. Chem. Phys. 35, 435 (1961).

Christ, C.L. Am. Min. 45, 334 (1960).

Christ, C.L.; Clark, Joan R. and Evans, H.T. Acta Cryst. 11, 761 (1958).

Cohen, M.H. and Reif, F. Solid State Phys. Vol. 5 (1957).

Cuthbert, J.D. and Petch, H.E. Jour. Chem. Phys. 38, 8, 1912 (1963).
Jour. Chem. Phys. 39, 5, 1247 (1963).

Dana, C.S.H. Manual of Mineralogy, 17th Edition (John Wiley & Sons).

Datars, R.D. M.Sc. Thesis, McMaster University (1956).

Edwards, J.O. and Ross, V. J. Inorg. Nucl. Chem. 15, 329 (1960).

Holuj, F. and Petch, H.E. Can. Jour. Phys. 34, 1169 (1956).
Can. Jour. Phys. 38, 515 (1960).

International Tables for Crystallography (1952).

Ito, T. and Mori, H. Acta Cryst. 6, 24 (1953).

Lal, K.C. and Petch, H.E. Jour. Chem. Phys. 40, 2741 (1964).

Petch, H.E.; Cranna, N.C. and Volkoff, G.M. Can. Jour. Phys. 31, 837 (1953).

Pennington, K.S. and Petch, H.E. Jour. Chem. Phys. 33, 2, 329 (1960).

Pennington, K.S. and Petch, H.E. Jour. Chem. Phys. 36, 5, 1216 (1962).
Jour. Chem. Phys. 36, 8, 2151 (1962).

Pound, R.V. Phys. Rev. 79, 685 (1950).

Purcell, E.M.; Torrey, H.C. and Pound, R.V. Phys. Rev. 70, 474 (1960).

Ross, V. and Edwards, J.O. Am. Mineral. 44, 875 (1959).

Schuster, N.A. Rev. Sc. Instr. 22, 254 (1951).

Volkoff, G.M.; Petch, H.E. and Smellie, D.W.L. Phys. Rev. 84, 602 (1951).
Can. J. Phys. 30, 270 (1952).

Volkoff, G.M. Can. J. Phys. 31, 820 (1953).

Waterman, H.H. and Volkoff, G.M. Can. J. Phys. 33, 156 (1955).

Whittaker, E. and Robinson, G. Calculus of Observations(Blackie & Sons Ltd., London 1948).